Measurement Science and Technology

PAPER • **OPEN ACCESS**

Electromagnetic immune phosphor-tipped fibre-optic thermometers

To cite this article: D H Lowe *et al* 2022 *Meas. Sci. Technol.* **33** 065007

View the article online for updates and enhancements.

You may also like

- Contactless temperature determination using dual-channel lock-in phosphor thermometry
Amir Hashemi, Gordana Jovicic, Miroslaw Batentschuk et al.
- Comparison of lifetime-based methods for 2D phosphor thermometry in high-temperature environment
Di Peng, Yingzheng Liu, Xiaofeng Zhao et al.
- Recent developments in phosphor thermometry
Andrew L Heyes and Frank Beyrau

This content was downloaded from IP address 202.8.112.115 on 16/06/2023 at 10:03

OPEN ACCESS
IOP Publishing
Measurement Science and Technology
Meas. Sci. Technol. **33** (2022) 065007 (8pp)
https://doi.org/10.1088/1361-6501/ac5440

Electromagnetic immune phosphor-tipped fibre-optic thermometers

D H Lowe[1,*], S L Andersen[2], G Sutton[1], J I Camacho[3], M B Copeland[3], H Kjeldsen[3] and K L Laursen[4]

[1] Department of Thermal and Radiometric Metrology, National Physical Laboratory, Teddington, United Kingdom
[2] Division of Environmental Technology, Danish Technological Institute, Aarhus C, Denmark
[3] Division of Energy and Climate, Danish Technological Institute, Aarhus C, Denmark
[4] Department of Medical Physics, Aalborg University Hospital, Aalborg, Denmark

E-mail: dave.lowe@npl.co.uk

Received 22 November 2021, revised 24 January 2022
Accepted for publication 9 February 2022
Published 7 March 2022

Abstract

Calibration traceability can be broken where there are significant, unquantified uncertainties. Thermometry in harsh environments using electrical sensors, such as thermocouples or resistance thermometers, can be unpredictably affected by electro-magnetic sources. For this application, phosphor based temperature sensors with fibre-optic connection have been made following two different approaches—phosphor decay time changes and phosphor emission spectral changes—and tested by bombardment with high energy electrons and by measurements in large magnetic fields. Both sets of tests showed good immunity to exposure, and with magnetic field tests significantly better than a thermocouple. Phosphor thermometry therefore has potential to retain traceability in situations where conventional sensors might fail.

Keywords: phosphor thermometry, electromagnetic immunity, calibration traceability

(Some figures may appear in colour only in the online journal)

1. Introduction

A measurement is only useful when it has an associated uncertainty: the range of values which could reasonably be attributed to that measurement [1]. In many cases there is a calibration chain with a primary standard at a national measurement institute (NMI) at one end and the actual measurement by a user at the other. Each step in the chain generally adds to the uncertainty, but provided the influencing factors are understood the end user can be confident that their measurement lies within the stated range of values.

There can be a big difference in the conditions at either end of the chain. The NMI environment is likely to be carefully controlled with specially designed and equipped laboratories to calibrate sensors with the smallest possible uncertainties. At the other end, things can be much less controlled, and some environments can potentially cause temporary or even permanent changes to the sensor output. Since there is always a need for sensors that are best suited to specific environments, it is one of the roles of an NMI to evaluate new approaches that might benefit end-users, usually with a view to improve their countries economy and competitiveness.

With thermometry, conventional electrical sensors such as thermocouples and resistance thermometers can be adversely affected and degraded when operated in hash environments.

* Author to whom any correspondence should be addressed.

Original Content from this work may be used under the terms of the Creative Commons Attribution 4.0 licence. Any further distribution of this work must maintain attribution to the author(s) and the title of the work, journal citation and DOI.

 © 2022 The Author(s). Published by IOP Publishing Ltd

Sensors can be perturbed by (a) electromagnetic (EM) fields [2] where electrical currents are capacitively or inductively coupled into the sensor circuit, producing errors which are difficult to quantify [3], or (b) damaged via transmutation when exposed to gamma or neutron fluxes [4]. For example, Type-K thermocouples were showed to exhibit substantial temperature errors due to the Ettingshausen–Nernst (EN) effect when exposed to large magnetic fields [5]—the EN effect produces an emf in an electrical conductor, such as a thermocouple, placed in a magnetic field and temperature gradient which are both transverse to the length of the wire.

Non-electrical sensors based on optical phenomena such as radiance, phosphorescence, reflectance and interference have the potential to overcome these challenges. By using optical fibres for such sensors, the conversion of optical to electrical signals, and the subsequent signal processing that is normally required, can be performed remotely away from the harsh environment.

As part of an EMPIR project [6], Denmark's Danish Technologicall Institute (DTI) and the UK's National Physical Laboratory (NPL) have each engineered phosphor-tipped fibre-optic temperature sensors, calibrated them and then tested them in harsh environments—DTI by bombarding with energetic electrons at Aalborg University Hospital (AUH) and NPL by testing in high magnetic fields.

2. Phosphor thermometry

Phosphor thermometry [7, 8] relies on photoluminescence—the emission of light at one wavelength caused by excitation at a different wavelength—where the luminescence has a temperature dependence. Thermographic phosphors are a type of photoluminescent material that continue to emit after the excitation stops and each has a characteristic, but temperature dependent, decay time. Switching the excitation off and measuring the decay constant allows the phosphor temperature to be determined. Alternatively, some photoluminescent materials (which may or may not also be phosphors) have a temperature dependent emission spectrum that can be measured under continuous excitation and, again, the material's temperature determined. Phosphor thermometry has been suggested for harsh environments where there are high electrical or magnetic fields [9, 10]. DTI and NPL used the same basic phosphor (manganese doped magnesium fluorogermanate, or MFG). This phosphor has a $^2E \rightarrow {}^4A_2$ energy states transition [11] with additional Stokes/anti-Stokes behaviour that results in a number of emission lines in the red part of the spectrum [12]. As well as a temperature dependence to the decay time, the relative intensity of the spectral emission peaks of this phosphor vary with temperature [13]. DTI measured the decay time of the broadband emission, while NPL measured relative changes of different emission lines.

2.1. Phosphor thermometer design—DTI

DTI used Mg4FGeO6:Mn thermographic phosphor. The temperature is determined from the decay time of the phosphor after excitation by a pulsed 415 nm LED light. The optical system is shown in figure 1. The sensor is composed of two separate aluminium-coated multimode fibres. The fibres have a stainless-steel flexible protection tube and are terminated by SMA connectors at one end. At the other end, the two fibres are inserted into a double-bore, open-end ceramic tube, which in turn is inserted into a 7 mm outer diameter single-bore closed-end ceramic tube with MFG-powder at the tip (figure 2). The optical fibre used for the sensor is a high-OH, 0.22 NA aluminium-coated step index multimode optical fibre from Thorlabs. The 400 μm core is made of pure silica with doped silica in the cladding. This fibre is rated for use up to 400 °C and it is this that determines the upper temperature limit of the probe. One end is protected by a stainless-steel flexible tube, and terminated by an SMA connector, while the other end is bare fibre. The two fibres are inserted into a double-bore open end ceramic tube, and the two fiber tips aligned with the open-end ceramic tube which is slowly lowered into a single-bore closed-end ceramic tube with phosphor at the tip. If the LED is on and the detection system is running while the inner tube is positioned in the outer tube, the intensity of the lifetime signal from the phosphor can be optimized. Figure 2 shows the light emitted from the MFG-powder inside the ceramic tube in the signal optimized position. The light from the LED is transmitted through one of the fibres to the phosphor, while the other fibre transmits the light emitted from the phosphor back to the optical measuring system and the detector for conversion into an electrical signal. The optical light detection and signal processing system setup is illustrated in figure 3.

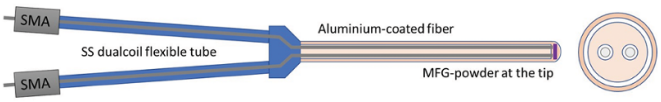

Figure 1. DTI phosphor thermometer sensor.

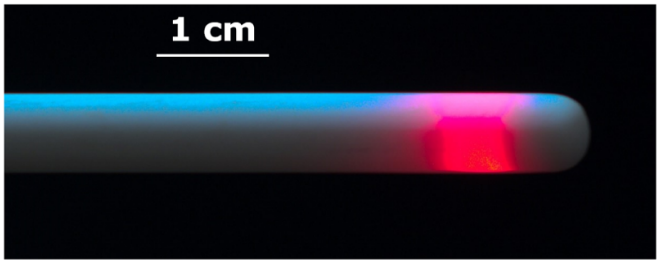

Figure 2. DTI sensor: the light emitted from the phosphor powder can be seen through the outer ceramic tube.

The LED is controlled by a fast LED driver and the blue electrical signal in the left graph of figure 3 represents the pulsed signal triggering the LED, which will quickly switch on and off and emit relatively sharp 50 ms long light pulses at 10 Hz. The light pulse is then transmitted to the MFG-powder at the tip of the sensor exciting the phosphor which will then start to emit light at peak wavelengths between 600 nm–700 nm. The emission of light from the phosphor will build up until the phosphor is fully saturated, as seen in the red curve of the graph in figure 3. To minimise the noise from

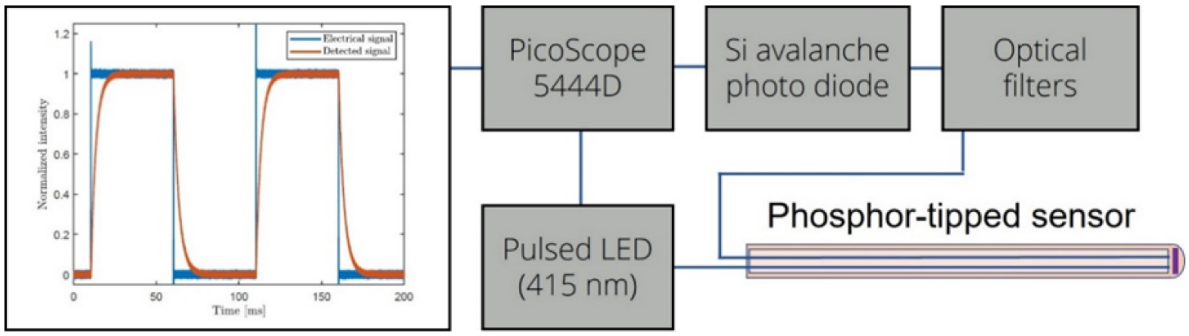

Figure 3. Setup of the DTI optical light detection and signal processing system. 415 nm pulsed light from and LED is transmitted via the optical fibre to the tip of the sensor, where the phosphor is excited to emit light in the wavelength range from 600 nm to 700 nm.

the surrounding light, a short-pass interference filter (cut-off wavelength 750 nm) and a long-pass filter (cut-off wavelength 650 nm) were installed before the silicon avalanche photo diode (Si APD). This type of detector was chosen for its high-speed detection of small signals in order to optimise the detection of light. This increases the upper temperature limit that can be achieved as the signal strength and lifetime both reduce as the phosphor gets hotter. The maximum electrical output signal from the Si APD is 2 V, and the signal is then captured in a fast, high-resolution oscilloscope (PicoScope 5444D), also chosen to enable detection of low-intensity light and thus temperature at high temperatures.

All the hardware is operated automatically in a LabVIEW program, which also automatically fits an exponential curve to the detected phosphor luminescence signal and estimates the temperature based on a calibration curve determined by an ITS-90 traceable calibration. The fitting routine first subtracts the background from the signal based on the average voltage reading from the detector in the oscilloscope as the signal from the phosphor has vanished completely. After background subtraction and adjustment of the trigger to follow the drop of the electrical signal ($t = 0$ is the time at which the phosphor excitation stops) a least-squares fit from $t = 0$ is performed to the equation

$$I = I_0 e^{-t/\tau} \tag{1}$$

where I_0 is the intensity of the signal at $t = 0$ and τ is the lifetime of the decay of the phosphors emission. The lifetime is extracted by the LabVIEW program and output to file at a rate of approximately 0.5 Hz. The temperature can thus be sampled at approximately this rate, and each reading of the thermometer uses one decay curve to measure the temperature. As the temperature of the phosphor is changed, the lifetime of the phosphor decay will change according to its dependency on the temperature, $\tau(T)$. The temperature dependency to be determined by calibration.

2.2. Phosphor thermometer design—NPL

The NPL design is described in detail in [13]. In brief, it uses a single 2 m multimode 400 µm core gold-coated fibre rated for use up to 750 °C. Figure 4 shows a schematic of

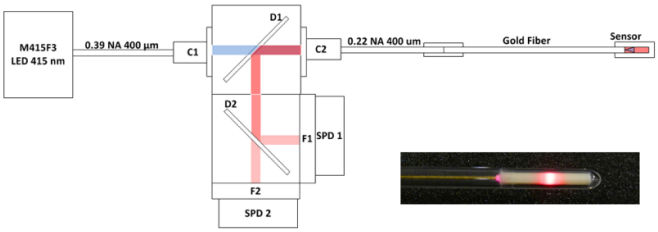

Figure 4. Schematic of the NPL system. The inset shows the energised sensor. Reproduced from [13]. © IOP Publishing Ltd. All rights reserved.

the NPL system. The MFG phosphor (Osram SV 067N) is excited by a Thorlabs M415F3 fibre coupled LED at nominally 415 nm into a 400 mm fibre. The collimators C1 and C2 are matched to couple the 0.39 numerical aperture (NA) input fibre to the 0.22 NA gold coated fibre. D1 and D2 are dichroic mirrors, F1 and F2 are interference bandpass filters and SPD1 and SPD2 are silicon photodetectors. The inset to figure 4 shows the energised sensor. Dichroic mirror D1 is used to separate the blue 415 nm fibre couple LED excitation from the red emitted light from the phosphor. The gold-coated fibre has a cleaved end which is embedded in phosphor powder, bonded in a 30 mm long 2.7 mm outer diameter alumina tube which forms the sensor. The sensor and gold-coated fibre are placed in a fused silica tube. The emitted light is further split with a second dichroic, D2, at 650 nm, the outputs are further filtered to give a channel at 630 nm and another at 660 nm, both 10 nm fwhm. Each channel is detected with a Hamamatsu S12915-1010R silicon photodiode with output current converted to voltage with NPL designed transimpedance amplifiers based on OPA129A op-amps with Caddock ultra stable low temperature coefficient resistors giving a gain for each channel of 10^7 V A^{-1}, 10^8 V A^{-1} or 10^9 V A^{-1}. The outputs from the amplifiers are connected to analogue inputs of an NI 6356-USB DAQ unit. The same unit provides the analogue square wave for the LED driver. A LabVIEW program runs the system and calculates temperature from the input voltages ratio. It is this ratio of the two channels, shown in figure 5, that is used to determine the temperature based on calibration. The channel signals start to drop rapidly as the temperature rises above about 400 °C as de-excitation of

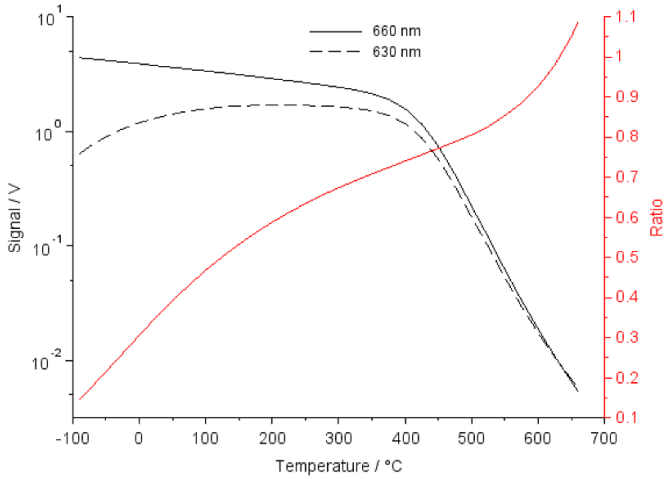

Figure 5. Channel signal levels (normalised to 10^7 V A^{-1}) and ratio of signals as a function of temperature for the NPL system. Reproduced from [13]. © IOP Publishing Ltd. All rights reserved.

the phosphor increasingly happens through thermal (phonon) processes rather than optical (photon) processes, however the sensitivity ($\Delta R/\Delta T$) increases as the absolute signals drop—the curve for ratio in figure 5 turns up progressively at higher temperatures. As a consequence, the thermometer is able to reach 660 °C—a useful value as that is the freezing temperature of aluminium used as one of the defining fixed-points of ITS-90—but at higher temperatures the signal is too noisy to be useful.

3. Calibration

3.1. DTI decay sensor

The calibration of the phosphor thermometer follows a standard procedure in an Ametek RTC-700 dry-block calibrator with digital load compensation to minimise the temperature gradient in the insert of the dry-block. In an automatic calibration setup (built in LabVIEW), the temperature of the calibrator is controlled automatically in steps of 20 °C, and the calibrator is allowed to stabilise before five consecutive lifetime spectra are acquired. The ITS-90 traceable temperature is found from the Pt-100 reference sensor inserted into the dry-block together with the phosphor thermometer as seen in figure 6(left). The reference sensor was calibrated in the dry-block calibrator according to the EURAMET Calibration Guide No. 13 Version 4.0 (09/2017). To estimate the variations in the performance of the phosphor thermometer (repeatability and reproducibility), the calibration of the thermometer was conducted three times under identical conditions and the two times where the sensor was removed from the dry-block calibrator and stressed slightly to simulate normal use. The result of the lifetime versus temperature measurement is shown in figure 7, where run 1–3 shows data for the repeatability (identical conditions) and run 4–5 shows data from the simulated use of the sensor.

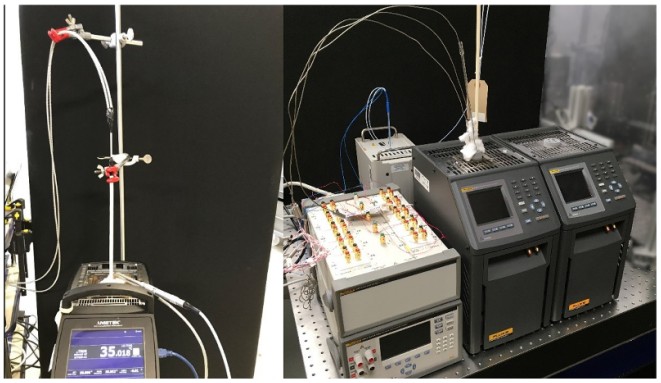

Figure 6. (left) DTI setup for calibration of the phosphor thermometer using a dry-block calibrator—calibration is done automatically using a LabVIEW program—and (right) NPL's calibration facility with programmable calibration sequence.

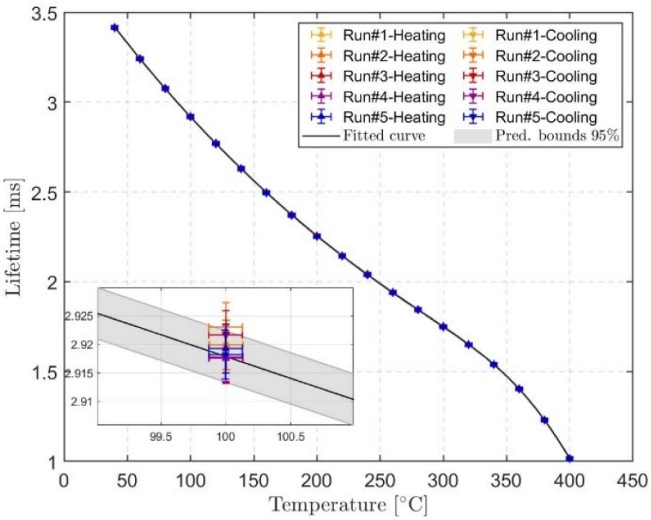

Figure 7. Calibration curve (temperature vs. lifetime) of the DTI phosphor thermometer with detail of the repeatability and the reproducibility.

Each calibration point has been established both during heating and cooling of the dry-block calibrator and a least-squares fit to all five sets of data has been made to the following equation

$$\tau(T) = \left[A \cdot e^{-BT} + C\right] \cdot \left[D - e^{-(E-T)^2/F^2}\right] \qquad (2)$$

where the coefficients A, B, C, D, E and F are the fitting coefficients and T is the temperature. This equation can reproduce the behaviour of the experimental data with good accuracy, as shown in figure 7. It was developed partly on the basis of expected physical behaviour and partly empirically. To evaluate the repeatability and the reproducibility of the sensor, the different cycles up and down in temperature (run 1–5) were compared to the fit of all the cycles. For a set of measured values, (T_i,τ_i) in run i, where T_i is the measured value of the reference sensor in the dry-block calibrator and τ_i is the

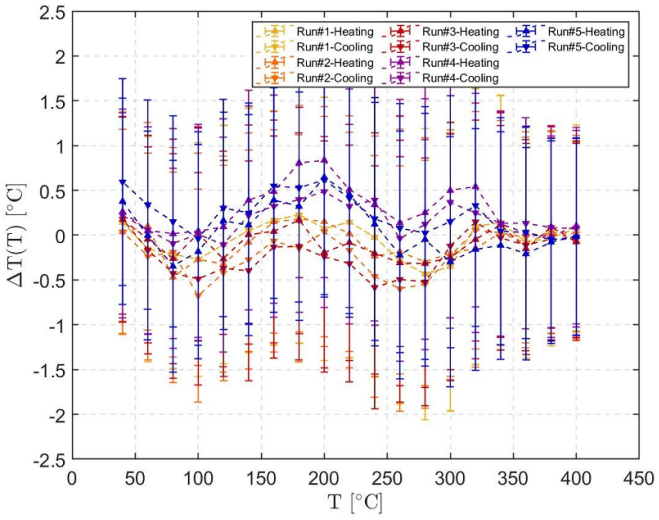

Figure 8. Calculated temperature equivalent of each run of the temperatures measured by the DTI sensor.

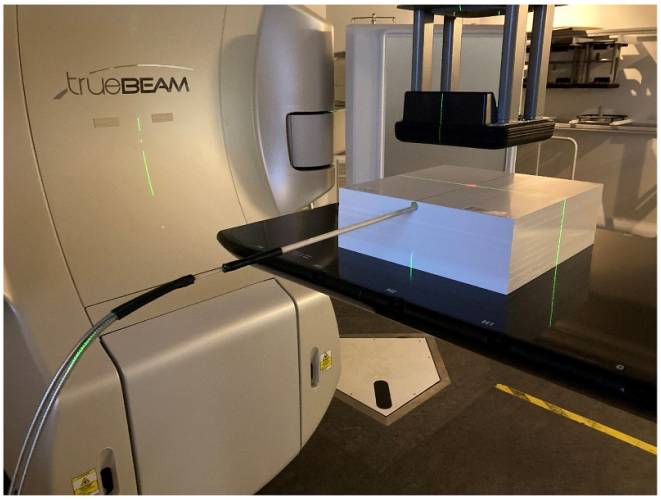

Figure 9. The setup at AUH to expose the DTI phosphor thermometer with 9 MeV and 20 MeV. The dose absorbed by the sensor is controlled by the thickness of solid water plates on top of the phosphor sensor.

corresponding value of the lifetime, the difference between the temperature achieved by applying the fitted reference function to the measured lifetime, $T_{cal}(\tau_i)$, and the temperature, T_i, of the dry-block reference is calculated using the following equation

$$\Delta T_i(T_i) = T_i - T_{cal}(\tau_i) = \frac{\tau_i - \tau_{cal}(T_i)}{\left(d\tau/dt(T_i)\right)_{cal}} \qquad (3)$$

Since the measured reference temperatures are equal within the uncertainty for all the runs 1–5, the calculation to the first order in the equation above is adequate. Figure 7 shows the calibration curve of the phosphor thermometer before electron exposure with five different runs to estimate the repeatability and the reproducibility of the sensor.

The calculations of $\Delta T_i(T_i)$ for each run up and down in temperature are shown in figure 8. As expected from the nature of the equation for $\Delta T_i(T_i)$, all the measurements are fluctuating around zero. The uncertainties given in the figure are calculated using error propagation and includes both standard uncertainties of the reference sensor and uncertainties in the estimation of the lifetime of the phosphor. The size of the fluctuations demonstrates the robustness of the phosphor thermometer and its ability to repeat and reproduce measurements of the temperature. Based on figure 8 the phosphor thermometer is shown to reproduce within ±2 °C including the uncertainties. In addition to the calculated uncertainties, a reproducibility contribution can be added when the sensor is used, and the drift between calculations should also be estimated.

3.2. NPL ratio sensor

Phosphor thermometers are calibrated at NPL using two Fluke dry block calibrators with reference thermometers calibrated in terms of ITS-90 (figure 6, right). One dry-block, with an NPL calibrated PT100 as reference, covers the range −45 °C to 100 °C. Another, with an NPL calibrated type-R thermocouple as reference, covers the range 50 °C–700 °C. A Thorlabs CCS-100 spectrometer allows phosphor emission spectra to be captured. Calibration of the NPL ratio thermometer in terms of ITS-90 has been described in detail elsewhere [13], including a complete uncertainty budget. In brief, its uncertainty ranges from about 1.5 °C at room temperature up to 4 °C at 650 °C at a confidence level of approximately 95% (that is, with a coverage factor $k = 2$). The uncertainties were evaluated with the thermometer making measurements at 1 Hz. The dominant uncertainty contributions were found to be the repeatability and hysteresis of the sensor, the interpolation between calibration points (based on a cubic spline) and the absolute accuracy of the voltage measurement.

4. Application in high EM environments

4.1. DTI phosphor thermometer electron exposure

To test the DTI phosphor thermometer's behaviour to a continuous flux of charged particles, the sensor was exposed to a well-characterised dose of 9 MeV and 20 MeV electrons, respectively, from a cancer treatment apparatus at Aalborg University Hospital.

Using a solid water phantom as build up material, the equipment was positioned at the water equivalent reference depth [14] for each electron energy. Absolute dose output at the depth of maximum expected dose was measured using a plane-parallel ionization chamber, and the percentage depth dose curve was utilised to calculate the absorbed dose at the reference depth. The setup is seen in figure 9. The sensor was exposed to 9 MeV and 20 MeV electrons, in turn, from the top and the thickness of the white solid water plates on top of the sensor is used to control the dose (more plates are needed for the higher energy electrons that penetrate deeper into the material). The solid water plates below the sensor are used to

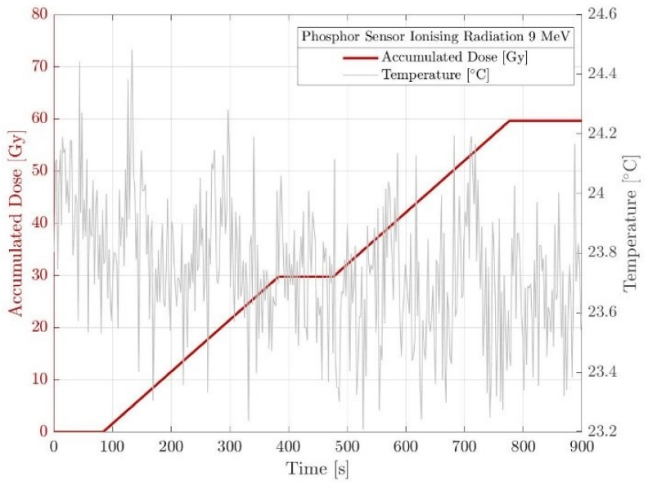

Figure 10. Temperature reading and absorbed dose during two times 300 s of exposure to 9 MeV electrons.

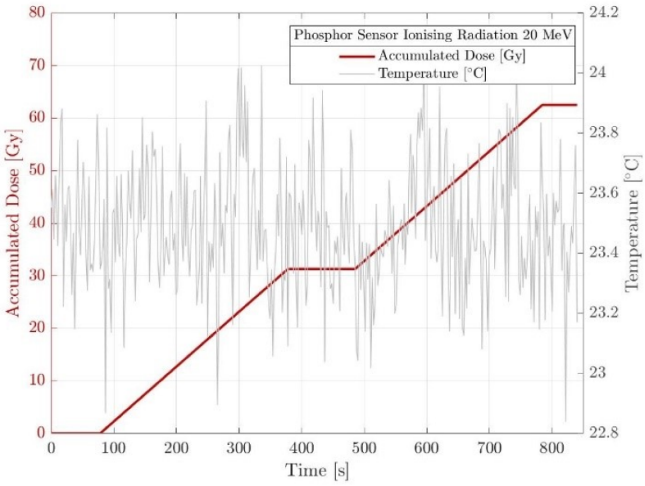

Figure 11. Temperature reading and absorbed dose during two times 300 s of exposure to 20 MeV electrons.

achieve optimal conditions for the backscattering of electrons to the sensor.

The phosphor sensor is connected to the optical light detection and signal processing system, which is located away from the electron beam to minimise the exposure from scattering electrons. The calibration coefficients are used in the phosphor thermometer to convert the measured lifetime into a temperature reading and measure the temperature during electron exposure. After approximately 80 s of stable baseline temperature logging, the electron beam is switched on and the sensor is exposed to 9 MeV and 20 MeV electrons, respectively, for 300 s. The beam is the switched off for 93 s (9 MeV) and 107 s (20 MeV) before being switched on again for 300 s more. The result of the electron exposure is seen in figure 10 (9 MeV electrons) and figure 11 (20 MeV electrons), the temperature reading as a function of time during exposure on the right axes. On the left axes is the accumulated absorbed dose of electrons at the depth of the sensor during the electron exposure. It is

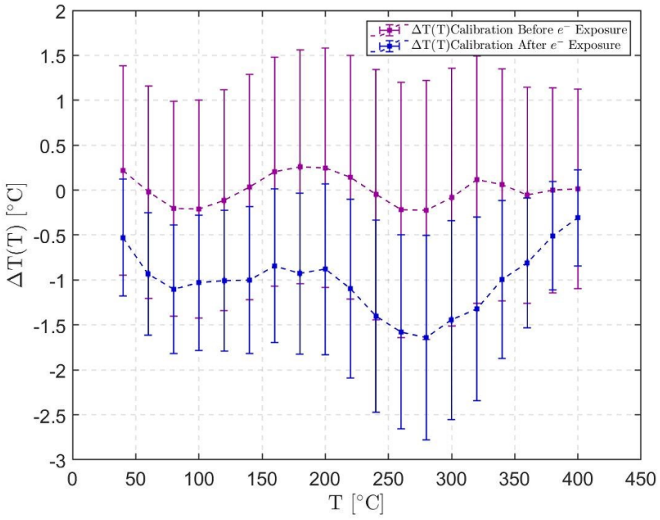

Figure 12. Difference between calibrations conducted before and after exposure from electrons of 9 MeV and 20 MeV.

clear from the data that there is no apparent impact of the thermometer reading to the exposure of electrons. After exposure with electrons at AUH, the thermometer was calibrated again. Looking at figure 12, which shows the change in ΔT from before and after exposure, it is clear the calibration has changed during electron exposure by -0.5 °C to -1.5 °C.

4.2. NPL phosphor thermometer magnetic field exposure

Tests were carried out comparing phosphor thermometer, type-R thermocouple and PT100 resistance thermometer. The thermocouple was made at NPL from 0.5 mm diameter nominally 99.99% wire in twin bore alumina. It had a bare junction in a silica tube—a metal sheaf which might have shielded the junction would be unsuitable in a magnetic field more than 2 T. The PT100 was an R-series from IST, 4-wire 2.8 mm diameter and 13 mm long.

Measurements were made at the NPL Electronic & Magnetic Materials Group, using a Bruker electromagnet capable of generating up to 3 T at the centre of the gap. Traceability for the magnetic field measurements is obtained via frequency using a nuclear magnetic resonance technique. Tests on smaller ac fields (to 20 mT) had shown that heating in the magnet coils and variation in laboratory temperature between tests would mask any small effects. Therefore, the three probes were mounted together between the poles of the Bruker electromagnet as shown in figure 13.

The electromagnet was cycled from 0 T to 2.3 T and back five times. It was apparent that there was a steady increase in ambient temperature during this time. To remove this drift a linear fit to each dataset was used as a baseline, and measurements were normalised to this reference. Figure 14 shows the change in measured temperature of the type-R thermocouple and phosphor thermometer with the changing magnetic field. As the field increases and decreases the measured temperature likewise increases and decreases by 0.6 °C. During zero field conditions the thermocouple reads the same as the phosphor

Figure 13. The three probes—NPL phosphor, thermocouple and resistance—mounted between the poles of the Bruker electromagnetic.

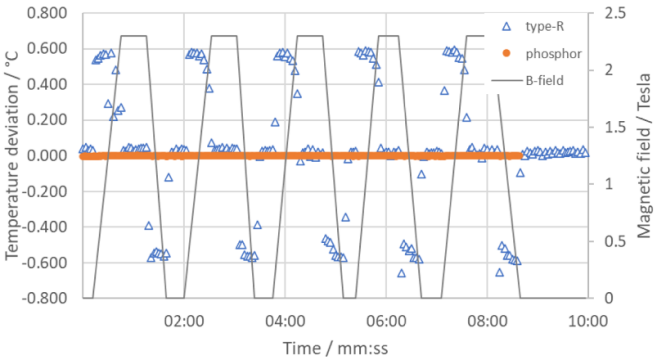

Figure 14. Deviation of the type-R thermocouple and NPL phosphor thermometer from base-line temperature as the magnetic field alternates between zero and 2.3 Tesla.

thermometer. The dominant effect is electrically-driven, not thermal, since when the B-field is reduced the thermocouple reads lower temperatures than the baseline corresponding to the temperatures measured at zero field. Figure 15 shows the equivalent situation with the PT100 resistance thermometer. In this case the PT100 reads high when the B-field is on, and possibly the phosphor thermometer does as well. It is noticeable that there is an overall change in the base-line from start to end, albeit only a few milli-Kelvin, but it does seem that something

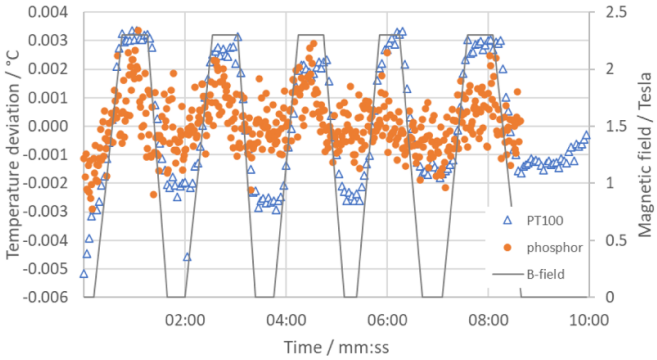

Figure 15. Deviation of the PT100 resistance thermometer and phosphor thermometer from base-line temperature as the magnetic field alternates between zero and 2.3 Tesla.

is getting warmed, possibly one of the sensors, when the field is on and that both the resistance and the phosphor thermometers are picking this up.

In terms of absolute temperature measurement and including calibration uncertainty, overall, the PT100 was $(20.33 \pm 0.04)\,^{\circ}\mathrm{C}$ and the phosphor thermometer was $(21.51 \pm 1.56)\,^{\circ}\mathrm{C}$ ($k = 2$). These agree within the uncertainties although it would have been nice to have better agreement.

5. Conclusions

Two designs of fibre-optic thermometer based on the thermographic phosphor MFG and the lifetime method (DTI) or ratio method (NPL) have been described. Calibration procedures for using dry-block calibrators have been developed, and traceability of the temperature measurements to the ITS-90 established.

The DTI thermometer was exposed to electrons of 9 MeV and 20 MeV for 10 min in total at each electron energy, and the effect of the ionising radiation evaluated. The total accumulated dose absorbed by the thermometer was approximately 60 Gy for the 9 MeV electrons and approximately 62 Gy for the 20 MeV electrons, and no change in the temperature reading by the thermometer was observed during exposure. However, as the re-calibration was conducted after the electron exposure, a change drift in the calibration curve of up to 1.5 °C was observed. Since no apparent change in the reading was seen during the exposure the change in the calibration curve could be due to other factors, and further investigation must be conducted to rule this out. Nevertheless, a reproducibility within ±3 °C for the present design of the DTI phosphor thermometer can be concluded.

The NPL thermometer was tested in a large (2.3 T) magnetic field and compared to a type-R thermocouple and PT100 4-wire resistance thermometer. The thermocouple showed significant changes of ±0.6 °C as the field changed, while the phosphor thermometer was comparably unaffected. Small changes at the level of 3 mK–5 mK were seen in both the PT100 and phosphor thermometer which may have been due to heating induced by the magnet.

We conclude that phosphor thermometers with calibration traceable to ITS-90 can be used in situations where more conventional sensors might be subject to unquantified errors that would break the chain of calibration traceability.

Data availability statement

The data that support the findings of this study are openly available at the following URL/DOI: https://doi.org/10.5281/zenodo.6260225.

Acknowledgments

This project has received funding from the EMPIR programme co-financed by the Participating States and from the European Union's Horizon 2020 research and innovation programme (Grant No. 17IND04).

The authors acknowledge and thank the help of Stuart Harmon, Connie Pallister, Darren Ryan, Adam Wilson and Frankie James of the NPL Electronic & Magnetic Materials Group.

ORCID iDs

D H Lowe https://orcid.org/0000-0003-1864-7139
G Sutton https://orcid.org/0000-0001-6753-2018

References

[1] JCGM 100:2008 2008 *Evaluation of Measurement Data—Guide to the Expression of Uncertainty in Measurement* (BIPM)
[2] Temperature measurement in electromagnetic environments *Technical Note* (available at: www.omega.co.uk/technical-learning/temperature-measurement-in-electromagnetic-environments.html)
[3] Chakraborty D and Brezovich I 1982 Error sources affecting thermocouple thermometry in RF electromagnetic fields *J. Microw. Power* **17** 17–28
[4] Giot M, Vermeeren L, Lyoussi A, Reynard-Carette C, Lhuillier C, Mégret P, Deconinck F and Gonçalves B S 2017 Nuclear instrumentation and measurement: a review based on the ANIMMA conferences *EPJ Nucl. Sci. Technol.* **3** 33
[5] Kollie T G, Anderson R L, Horton J L and Roberts M J 1977 Large thermocouple thermometry errors caused by magnetic fields *Rev. Sci. Instrum.* **48** 501
[6] European Metrology Programme for Innovation and Research Enhancing process efficiency through improved temperature measurement 2 *Project Number* 17IND04 (available at: www.euramet.org/research-innovation/search-research-projects/details/project/enhancing-process-efficiency-through-improved-temperature-measurement-2/)
[7] Allison S W and Gillies G T 1997 Remote thermometry with thermographic phosphors: instrumentation and applications *Rev. Sci. Instrum.* **68** 2615
[8] Khalid A H and Kontis K 2008 Thermographic phosphors for high temperature measurements: principles, current state of the art and recent applications *Sensors* **8** 5673–744
[9] Fouliard Q, Hernandez J, Heeg B, Ghosh R and Raghavan S 2020 Phosphor thermometry instrumentation for synchronized acquisition of luminescence lifetime decay and intensity on thermal barrier coatings *Meas. Sci. Technol.* **31** 054007
[10] Cai T, Mohammadshahi S, Lee T and Kim K 2021 Simultaneous measurement of two-dimensional temperature and strain fields based on thermographic phosphor and digital image correlation *Meas. Sci. Technol.* **32** 095204
[11] Brubach J, Feist J P and Dreizler A 2008 Characterization of manganese-activated magnesium fluorogermanate with regards to thermographic phosphor thermometry *Meas. Sci. Technol.* **19** 025602
[12] Adachi S 2020 Review—Mn^{4+}-activated red and deep red-emitting phosphors *ECS J. Solid State Sci. Technol.* **9** 016001
[13] Lowe D, Sutton G, Sposito A, Machin G and Pearce J 2021 Design, construction and traceable calibration of a phosphor-based fibre-optic thermometer from 0 °C to 650 °C *Meas. Sci. Technol.* **32** 094004
[14] International Atomic Energy Agency 2000 Absorbed dose determination in external beam radiotherapy *Technical Reports Series No.* 398